HHS Public Access

Author manuscript

Arterioscler Thromb Vasc Biol. Author manuscript; available in PMC 2020 May 01.

Published in final edited form as:

Arterioscler Thromb Vasc Biol. 2019 May ; 39(5): 902–914. doi:10.1161/ATVBAHA.118.312301.

Atheroprotective Flow Upregulates ITPR3 in Vascular Endothelium via KLF4-Mediated Histone Modifications

Ming He, MD, PhD[*], **Tse-Shun Huang, PhD**[*], **Shuai Li, PhD**, **Hsiao-Chin Hong, PhD**, **Zhen Chen, PhD**, **Marcy Martin, PhD**, **Xin Zhou, PhD**, **Hsi-Yuan Huang, PhD**, **Shu-Han Su, PhD**, **Jiao Zhang, MD, PhD**, **Wei-Ting Wang, PhD**, **Jian Kang, PhD**, **Hsien-Da Huang, PhD**, **Jin Zhang, PhD**, **Shu Chien, MD, PhD**[†], and **John Y-J. Shyy, PhD**[†]

Department of Medicine (M.H., S.L., H.-C.H., Z.C., M.M., H.-Y.H., S.-H.S., Jiao Zhang, W.-T.W., J.K., S.C., J.Y-J.S.), Department of Bioengineering and Institute of Engineering in Medicine (T.-S.H., S.C.), Department of Pharmacology (X.Z., Jin Zhang.), University of California, San Diego, and Institute of Bioinformatics and Systems Biology (H.-C.H., H.-Y.H., H.-D.H.), Department of Biological Science and Technology (W.-T.W.), National Chiao Tung University, Hsin-Chu, Taiwan

Abstract

Objective: The topographic distribution of atherosclerosis in vasculature underscores the importance of shear stress in regulating endothelium. With a systems approach integrating sequencing data, the current study aims to explore the link between shear stress-regulated master transcription factor and its regulation of endothelial cell (EC) function via epigenetic modifications.

Approach and Results: H3K27ac-ChIP-seq, ATAC-seq, and RNA-seq were performed to investigate the genome-wide epigenetic regulations in ECs in response to atheroprotective pulsatile shear stress (PS). *In silico* prediction revealed that KLF4 binding motifs were enriched in the PS-enhanced H3K27ac regions. By integrating PS- and KLF4-modulated H3K27ac, we identified 18 novel PS-upregulated genes. The promoter regions of these genes showed an overlap between the KLF4-enhanced ATAC signals and the PS-induced H3K27ac peaks. Experiments using ECs isolated from mouse aorta, lung ECs from EC-KLF4-TG vs. EC-KLF4-KO mice, and atorvastatin-treated ECs showed that ITPR3 was robustly activated by KLF4 and statins. KLF4 ATAC-qPCR and ChIP-qPCR further demonstrated that a specific locus in the promoter region of the *ITPR3* gene was essential for KLF4 binding, H3K27ac enrichment, chromatin accessibility, RNA polymerase II recruitment, and ITPR3 transcriptional activation. Deletion of this KLF4 binding locus in ECs by using CRISPR-Cas9 resulted in blunted calcium influx, reduced expression of endothelial nitric oxide synthase, and diminished NO bioavailability.

[†]Correspondence: John Y-J. Shyy, Ph.D., Department of Medicine, University of California, San Diego, 9500 Gilman Dr., La Jolla, CA 92093-0613, USA. Tel: 858-534-3736, jshyy@ucsd.edu, or, Shu Chien, M.D., Ph.D., Department of Bioengineering, University of California, San Diego, 9500 Gilman Dr., La Jolla, CA 92093-0412, USA. Tel: 858-349-5296, shuchien@ucsd.edu.

[*]Ming He and Tse-Shun Huang contributed equally to this work.

Disclosures

None.

Conclusions: These results from a novel multi-omics study suggest that KLF4 is crucial for PS-modulated H3K27ac that allow the transcriptional activation of ITPR3. This novel mechanism contributes to the Ca^{2+}-dependent eNOS activation and EC homeostasis.

Keywords

shear stress; histone modifications; KLF4; ITPR3; eNOS

Subject codes

Vascular Biology; Hemodynamics; Gene Expression and Regulation; Epigenetics; Endothelium; Vascular Type; Nitric Oxide

Introduction

Distinct flow patterns cause different gene expression profiles in vascular endothelial cells (ECs), which lead to variations in atheroprotective vs. atheroprone phenotypes[1–3]. Previous studies with the use of microarray and RNA-seq have generated a plethora of data to decipher gene expression profiles in ECs in response to atheroprotective vs. atheroprone flows[4–6]. In principle, the atheroprotective flow pattern upregulates genes that are anti-inflammatory and anti-oxidative and enhance nitric oxide (NO) bioavailability. In contrast, atheroprone flow impairs EC function by inducing genes that increase the inflammatory and oxidative burden[7].

Recent advances in studies on mechanotransduction have revealed that epigenetics, including DNA methylation, histone modifications, and long non-coding RNAs, are integral to shear-stress–regulated gene expression[8–12]. Covalent modifications of histones at adjacent regions of encoded genes govern the status of transcription[13]. For example, mono-methylation of histone 3 lysine 4 (H3K4me1) marks the *loci* as poised, whereas acetylation of H3K27 (H3K27ac) results in a loosely packed euchromatic state, which allows for access by transcription factors (TFs) and recruitment of RNA polymerase II (Pol II) to initiate transcription[14]. Pioneer TFs bind to the condensed chromatin to modify chromatin accessibility, thereby facilitating the recruitment and binding of other TFs and the transcriptional machinery[15].

The emerging techniques of next-generation sequencing (NGS), including chromatin immunoprecipitation followed by high throughput sequencing (ChIP-seq) and assay for transposase-accessible chromatin-seq (ATAC-seq), allow for studying epigenetic regulation at the genome-wide level[16,17]. Transcriptionally activated *loci*, defined by H3K4me1+/H3K27ac+[18], at the basal state in human umbilical vein ECs (HUVECs) have been profiled in the ENCODE project (Histone Modifications by ChIP-seq from ENCODE/Broad Institute, GSE29611)[19]. By using ChIP-seq and ATAC-seq, the current study aimed to explore the link between epigenetic regulation and gene expression in ECs responding to distinct flow patterns. Such analyses revealed that Krüppel-like factor 4 (KLF4) functions as a pioneer TF in ECs to de-condense chromatin, thus allowing for transcriptional activation of atheroprotective flow-responsive genes, exemplified by inositol 1,4,5-trisphosphate (IP_3) receptor 3 (*ITPR3*) encoding ITPR3.

In ECs, intracellular calcium concentration ($[Ca^{2+}]_i$) can be regulated in part by the release of calcium from ITPR stores[20]. There is substantial evidence that the activation of the IP_3-ITPR pathway, with an ensuing increase in $[Ca^{2+}]_i$, leads to increased production of NO via activated endothelial nitric oxide synthase (eNOS), thereby inducing the relaxation of vascular smooth muscle cells[21,22]. $[Ca^{2+}]_i$ has been reported to be modulated by ITPR1 in ECs and ITPR2 in cardiomyocytes to maintain normal blood pressure and regulate mitochondrial function, respectively[22,23]. The Human Protein Atlas project (www.proteinatlas.org) demonstrated that among ITPR family members, ITPR3 is predominantly expressed in ECs[24]. However, the epigenetic and transcriptional regulation of ITPR3 is largely unknown. Our data from high-throughput unbiased profiling (i.e., ChIP-seq, ATAC-seq, and RNA-seq) followed by functional validation demonstrate that atheroprotective flow is a principal mechanosensitive cue for activating the ITPR3-eNOS axis in ECs via KLF4-regulated ITPR3 transcription.

Material and Methods

The authors declare that all supporting data are available within the article and its online supplementary files. The associated ChIP-seq and ATAC-seq data have been made publicly available at the NCBI's GEO and can be accessed at https://www.ncbi.nlm.nih.gov/geo/query/acc.cgi?acc=GSE128391

Cell culture, shear stress, and antibodies

HUVECs were obtained from Cell Applications (San Diego, CA) and were maintained and exposed to shear stress as previously described[32]. Briefly, a circulating flow system was used to impose atheroprotective pulsatile shear stress (PS, 12 ± 4 dyn/cm^2) or atheroprone oscillatory shear stress (OS, 1 ± 4 dyn/cm^2). The flow system was held at 37°C and ventilated with 95% humidified air plus 5% CO_2. Antibodies against H3K4me1 and H3K27ac were from Active Motif (Carlsbad, CA); anti-eNOS, anti-phospho-eNOS (Ser1177), and anti-calmodulin antibodies were from Abcam (Cambridge, MA); anti-α-tubulin, anti-phospho-eNOS (Thr495), and horseradish peroxide-conjugated anti-rabbit and anti-mouse antibodies were from Cell Signaling Technology (Beverly, MA); anti-caveolin-1 antibody was from Santa Cruz Biotechnology (Santa Cruz, CA). The atorvastatin hemicalcium salt was from Tocris Biosciences (Bristol, UK).

ChIP-seq, RNA-seq, and ATAC-seq

Cells were fixed at 37°C with 1% paraformaldehyde for 15 min, and then washed twice in cold phosphate buffered saline (PBS) and scraped and pelleted at 3000 rpm for 5 min; cell pellets were resuspended in 50 μl lysis buffer, then diluted with 500 μl TE buffer before sonication. For antibody and chromatin binding, 20 μg chromatin, 3 μg antibody, and 11 μl dynabeads (Thermo Fisher Scientific, Waltham, MA) were incubated in a master mix buffer at 4°C overnight. The chromatin were eluted by 150 μl elution buffer followed by crosslinking at 65℃ overnight. After incubation with RNase A and Proteinase K, DNA was precipitated by phenol:chloroform:isoamyl (25:24:1, v/v), dissolved in TE buffer, and stored at −80°C. For RNA-seq, total RNA from HUVECs was extracted by using the mirVana miRNA Isolation Kit (Thermo Fisher) according to the manufacturer's instructions. For

ATAC-seq, ECs were washed twice with cold PBS, and nuclei were isolated by resuspending ~5000 cells in 50 μl cold lysis buffer (10 mM Tris-HCl, 10 mM NaCl, 3 mM MgCl2, and 0.1% NP-40). The nuclear pellets were resuspended in 50 μL transposition buffer (Nextera DNA Library Preparation Kit (Illumina Inc. San Diego, CA) and 22.5 μL H_2O, and then incubated at 37°C for 30 min. After incubation, the DNA samples were purified with Qiagen MinElute PCR purification kit. The preparation of the various sequencing libraries and sequencing by use of an Illumina HiSeq 2000 sequencer were performed in the IGM Genomics Core, University of California, San Diego. The resulting sequencing raw data have been made publicly available at the NCBI's GEO (accession No. GSE128391).

Analysis of sequencing libraries

Trimmomatic v0.35 was used to process the fastq files to remove poor-quality and adapter reads[26]. RNA reads were aligned by using HISAT2 with a pre-built reference human UCSC hg19 transcriptome index[27]. To evaluate gene expression, gene information was obtained from GENCODE (https://www.gencodegenes.org/, version GRCh37) and count per gene was calculated by featureCount[28]. Statistics analysis of differentially expressed genes was performed with the use of DESeq2 to process the raw counts of genes[29]. We used Benjamini-Hochberg method at level of $q<0.01$ to limit false positive rate in multiple testing. DNA reads were aligned to the pre-built UCSC hg19 reference human genome index by bowtie2[30]. For DNA alignment, PCR duplicate reads were further removed by Picard-tools (https://broadinstitute.github.io/picard/). To identify ChIP- and ATAC-enriched *loci*, the de-duplicated alignments were subjected to peak calling and annotated by the homer suite[31]. Homer-idr (https://github.com/karmel/homer-idr) was used to process ChIP-seq data for high reproducibility among biological duplicates. *Loci* with overlapped ChIP-seq and ATAC-seq data were identified by bedtools (http://bedtools.readthedocs.io/en/latest/). The resulting profiles were visualized by use of the UCSC genome browser (https://genome.ucsc.edu). To identify ChIP/ATAC read enrichment, the identified peaks were split into 500-bp windows and processed by featureCount and DESeq2. Heatmaps and binding profiles of ChIP- and ATAC-seq data were generated by using deeptools[32].

Motif analysis

To define enriched TF binding sites, RSAT Metazoa was used to process H3K27 hyperacetylated *loci* identified in ChIP-seq analysis[33]. Genomic sequences of PS and OS *loci* were fetched separately and used as mutual background models in the peak-motif program of RSAT. The motifs enriched by PS or OS vs. background model were corrected for positional bias and then output for follow-up analyses.

RT-qPCR, western blot analysis, and RNA silencing

Total RNA was isolated from cultured ECs, mouse lung ECs, and the intima of the mouse aorta, aortic arch, and thoracic aorta by using Trizol reagent (Invitrogen) and protein was isolated with RIPA lysis buffer. Animal experiments were approved by the institutional animal care and use committee of the University of California, San Diego. C57BL/6j mice were obtained from The Jackson Laboratory (Sacramento, CA). At 6–8 weeks of age, both sexes (3 male and 3 female) of mice were intraperitoneally injected with atorvastatin (50 mg/kg) or an equal volume of saline (500 μL) randomly. After 24 hr, mice were sacrificed by

CO2 inhalation, lung ECs were harvested for RNA isolation. For intimal mRNA isolation, the aortic arch (AA) and thoracic aorta (TA) were isolated and peri-adventitial fat was removed, the aortic lumen was quickly flushed with 250 μl TRIzol reagent with use of a 28 1/2-gauge syringe. Due to the limited amount of mRNA that can be extracted from TA and AA, the intimal eluates from five C57BL/6j mice (3 male and 2 female) were collected and pooled for RNA isolation. The small number of animals used for isolating intimal mRNA limited the separation of male and female mice for tissue collection. Total RNA from lung ECs of EC-KLF4$^{-/-}$ and EC-KLF4-Tg mice was a gift from Dr. Mukesh K. Jain[34]. The extracted RNA was reverse-transcribed and analyzed by qPCR with β-actin as an internal control. The primer sequences used for qPCR are in Supplemental Table 2. For western blot analysis, protein extracts were separated by SDS-PAGE and transferred to PVDF membranes, which were incubated with primary antibodies. Protein bands were detected by using Immobilon chemiluminescent substrate (Millipore). Human THBD, DAG1, CAMKKα, ITGB4, ALS2CL, and ITPR3 siRNA and control siRNA (Ctrl siRNA) were obtained from Qiagen. All RNAs were transfected into ECs by using Lipofectamine RNAi max (Invitrogen).

Immunostaining and eNOS activity assay

ECs were fixed in 4% paraformaldehyde at 4°C for 10 min. Triton X-100 (0.1% in PBS) was then added. Specimens were then incubated with primary antibody for 1 hr, then for 2 hr with Alex-488 (anti-mouse)- or Alex-568 (anti-rabbit)-conjugated secondary antibody. Fluorescent images were acquired under an Olympus FV100 confocal microscope. The colocalization of eNOS and caveolin-1 was quantified by Image J. NO production was assessed as nitrite (NO^{2-}) accumulated in culture media by nitrite/nitrate fluorometric assay (Cayman Chemicals).

CRISPR/Cas9-mediated KLF4 binding site disruption

Single-guide RNAs (sgRNAs) were designed by using the online tool provided by the Church laboratory[35]. Oligonucleotide pairs with BsmBI-compatible overhangs were annealed and cloned into the lentiviral vector lentiCRISPR v2 (Addgene plasmid #52961)[36]. For virus production, HEK293T cells were transfected with lentiCRISPR v2, psPAX2 (Addgene #12260) and pMD2.G (Addgene plasmid #12259) at a 8:4:1 ratio with 100 μl Plus Reagent (Life Technologies) and 50 μl Lipofectamine 2000 (Life Technologies) and cultured in Dulbecco's modified Eagle medium supplemented with 10% fetal bovine serum, 1% sodium pyruvate, 1% non-essential amino acids, 1% kanamycin, 50 units/ml penicillin/streptomycin and 50 μM β-mercaptoethanol for 48 hr before cell lysis. Cell debris was removed by centrifugation followed by ultra-centrifugation (2.5 hr at 24,000 rpm) with a sucrose cushion. Early passage HUVECs were lentivirally transduced and cultured for 2 days in medium supplemented with 1 μg/ml puromycin to select cells expressing the lentiCRISPR V2 vector. A mixed population of lentiCRISPR V2–positive ECs was selected.

Calcium imaging

For Fura2-AM experiments, cells were pre-incubated with 0.5 μM Fura2-AM (Molecular Probes) for 15 min at 37°C before imaging. Cells were washed twice with modified HBSS and imaged in the dark at room temperature. Images were acquired under a Zeiss Observer

Z1 microscope with a cooled charge-coupled device camera (Roper). Fura2 dual excitation ratio imaging involved two excitation filters, ET340x and ET380x for 340-nm and 380-nm excitation, and a HQ535/45m emission filter. Exposure times were 200 ms, and images were taken every 30 s. Imaging data were analyzed with Metafluor 6.2 software (Universal Imaging). Fluorescence images were background-corrected by deducting the background (regions with no cells) from the emission intensities of cells loaded with Fura2-AM. The 340/380-nm emission ratio was calculated at different times. Traces were normalized by setting the emission ratio to 1 before the addition of drugs.

Statistical analysis

All statistical analyses were performed using SPSS version 14.0 or R project version 2.10. Statistical analyses of sequencing data were performed using standard codes for the packages indicated above. Wet bench experiments results were expressed as means ± SEM. Initially, data were tested for normality and equal variance to confirm the appropriateness of parametric tests. Parametric data was analyzed by 2-tailed Student's *t* test. If normality or equal variance test failed, non-parametric data were analyzed using Kruskal-Wallis with Dunn's post hoc test or 2-tailed Mann-Whitney U test. $P < 0.05$ was considered statistically significant.

Results

Shear stress regulation of histone modifications

ECs subjected to atheroprotective PS or atheroprone OS were used for H3K4me1 ChIP-seq and H3K27ac ChIP-seq to explore the histone modifications in ECs responding to distinct flow patterns. We first identified the *cis*-elements involved in the active chromatin state at the genome-wide scale, represented by H3K4me1+/H3K27ac+ signals. Because H3K4me1+ is a prerequisite for the active *cis*-element and H3K27ac+ is more prominent for defining the activated chromatin state[18], we quantified the chromatin activation by assessing the acetylation level of H3K27 (i.e., H3K4me1+/H3K27ac^{high} vs H3K4me1+/H3K27ac^{low}), which depicts a chromatin relaxation state with the ensuing transcriptional activation[37]. Changes in H3K27ac levels were then cross-referenced with those from RNA-seq expression profiles under PS or OS for exploring the expression of genes regulated by the active chromatin state. Fig. 1A shows the heatmap generated from such analysis and includes genes that showed both enriched H3K27ac+ and higher RNA levels. As positive controls, PS-responsive genes such as *NOS3* (encoding eNOS) and *KLF4* showed enhanced H3K27ac signals in their promoter regions under the PS condition. Conversely, OS-induced genes such as selectin E (*SELE*; encoding E-selectin) and vascular cell adhesion protein 1 (*VCAM1*) showed enhanced H3K27ac signals in their promoter regions under the OS condition (Fig. 1B). These flow-induced H3K27ac *loci* overlapped with those defined in ENCODE data for static HUVECs (GSM733691)[38]. The H3K27ac enrichment in the promoter regions of *NOS3*, *KLF4*, *SELE*, and *VCAM1* (highlighted in green in Fig. 1B) in ECs was indeed regulated by shear stress, as verified by H3K27ac ChIP-qPCR (Fig. 1C).

To deduce the TFs involved in the transcription of these differentially regulated genes under PS vs. OS, we analyzed TF binding sequences located at these differentially enriched

H3K27ac *loci*. Sp1-like/KLF family and FOX/CPEB binding sequences were among the top-ranked *cis*-elements involved in PS- and OS-enriched H3K27ac *loci*, respectively (Fig. 1D). KLF4 is a master regulator of EC homeostasis that is PS-inducible. As a pioneer TF, KLF4 recruits histone acetyltransferases and deacetylases to modify histones, thereby changing the chromatin accessibility[39]. Thus, we used data from ATAC-seq to compare the chromatin accessibility in control ECs and ECs overexpressing KLF4. The *loci* close to the KLF4 binding sites were largely less condensed in ECs overexpressing KLF4 (Fig. 2A), suggesting that KLF4 increased the chromatin accessibility of its targeted genes. In line with the GC-enriched KLF4 binding sequence shown in Fig. 1D, the GC content and percentage of KLF4 binding sites were higher in these decondensed *loci* of PS-inducible genes, than that of PS-suppressed or non-effected genes (Fig. 2B). Such enrichments were not found in binding sequence for other GC-bound TFs such as ZEB1 and SNAI2 (Fig. 2C). The KLF4-decondensed *loci* had a higher degree of superimposition with the PS-enriched H3K27ac *loci* than those of OS-enriched H3K27ac (Fig. 2D). Furthermore, ectopically expressed KLF4 decondensed ~25% of the PS-enhanced H3K27ac *loci*, as revealed by superimposing the Ad-KLF4-ATAC and H3K27ac ChIP-seq data (Fig. 2E). These results confirmed that KLF4 is a pioneer TF in ECs that regulates multiple PS-responsive genes via chromatin remodeling.

PS-induced transcription via KLF4

Next, we set three criteria to screen the PS-inducible genes via KLF4 regulation: (1) inducible by PS, as revealed by RNA-seq; (2) containing putative KLF4 binding sites in the promoter region; and (3) containing enhanced H3K27ac signal near the KLF4 binding sites under PS (Fig. 3A). Consequently, we selected 18 genes that were putatively induced by PS via KLF4 (Table 1). We first examined the dynamic regulation of these 18 genes by PS vs. OS in time-series RNA-seq[6]. From these 18 genes, all showed higher expression under PS than OS except for ST6GAL1 and TBC1D7 (Fig. 3B and Sup. Fig. 1). As positive controls, *KLF4* and *NOS3* (encoding eNOS), known to be PS-responsive, were substantially induced by PS for up to 24 hr. Next, these 18 genes were found to have at least one putative KLF4 binding site in the promoter regions, with H3K27ac enrichment in the flanking region (Fig. 3C and Sup. Fig. 2A). Further validation by Ad-KLF4-ATAC-seq revealed that the promoter regions of these 18 genes had a KLF4-enhanced ATAC signal in at least one set of ATAC-seq data (Fig. 3D and Sup. Fig. 2B). Importantly, these enhanced ATAC signals had considerable overlap with the PS-induced H3K27ac peaks.

The tunica intima tissue isolated from the thoracic aorta (TA, atheroprotective region) and aortic arch (AA, atheroprone region) of C57BL/6j mice was used first for biological validation. Overall, the mRNA level for 16 of the 18 genes was higher in TA than AA intima (Fig. 4A). The cholesterol-lowing drugs statins have a profound effect on maintaining a functional endothelium and have been shown to induce KLF4 in ECs *in vitro* and *in vivo*[40]. Atorvastatin treatment of cultured ECs for 48 hr induced 9 of the 18 genes (Fig. 4B). Furthermore, 12 genes were significantly induced in lung ECs isolated from mice receiving atorvastatin for 3 days (Fig. 4C). To explore the KLF4 inducibility, we overexpressed KLF4 in cultured ECs and examined the mRNA level of the 18 genes. Eight genes were induced by KLF4 overexpression (Fig. 4D). For *in vivo* validation of KLF4 induction of these genes,

lung ECs were isolated from EC-KLF4-Tg and EC-KLF4$^{-/-}$ mice[34]; 12 of the 18 genes were induced in a KLF4-dependent manner *in vivo* (Fig. 4E). Overall, 6 genes in ECs, viz. *CAMKK1, DAG1, THBD, ITPR3, ALS2CL, and ITGB4*, were commonly induced by PS, atorvastatin, and KLF4 *in vitro* and *in vivo*.

ITPR3 regulation of eNOS in ECs

We next explored whether changes in the expression of these 6 genes affected EC functions by using eNOS-derived NO bioavailability as a functional readout. ECs in which the 6 commonly induced genes had been individually knocked down were treated with atorvastatin or PS for 16 hr. eNOS expression and NO production was assessed accordingly. siRNA knockdown of ITPR3 or ALS2CL attenuated the atorvastatin- or PS-induced eNOS mRNA level in ECs (Fig. 5A). However, ITPR3 knockdown impaired the atorvastatin-increased NO production more drastically and hence we focused on ITPR3 for further functional characterization (Fig. 5B).

A hallmark of eNOS activation is its phosphorylation at Ser-1177[41,42]. Concurrently, eNOS Thr-495 dephosphorylation is positively associated with stimuli that elevate $[Ca^{2+}]_i$[43]. siRNA knockdown of ITPR3 impaired the eNOS Ser-1177 phosphorylation increased by atorvastatin and PS (Fig. 5C, 5D). As well, ITPR3 knockdown abolished the eNOS Thr-495 dephosphorylation in response to atorvastatin or PS (Fig. 5C, 5D). *In vivo*, the differential regulation of ITPR3 by atheroprotective vs. atheroprone flows was evident by a higher level of ITPR3 in the TA than AA region (Fig. 5E). The increased ITPR3 expression was also accompanied by decreased eNOS Thr-495 phosphorylation and increased Ser-1177 phosphorylation and eNOS level (Fig. 5E).

Functioning as a calcium channel on the ER membrane, ITPR regulates $[Ca^{2+}]_i$[44]. ITPR3 knockdown indeed decreased the ionomycin- and PS-induced calcium influx in ECs (Fig. 5F, 5G). Changes in $[Ca^{2+}]_i$ modulate eNOS phosphorylation status and also eNOS subcellular compartmentation in ECs, which plays an essential role in regulating eNOS activity[43,45]. The underlying mechanism involves the disassembly of the eNOS–caveolin-1 (Cav-1) complex in the lipid raft and assembly of the eNOS–calmodulin complex in the non-lipid raft (illustrated in Fig. 5J). With atorvastatin treatment of wild-type ECs, eNOS was translocated from lipid rafts to non-lipid rafts. This was revealed by the dissociation of eNOS from Cav-1[46], a structural protein in caveolae, and the association with calmodulin (lane 2 vs 1 in Fig. 5H). Notably, such eNOS translocation and eNOS-calmodulin association were not seen in ECs with ITPR3 knocked down (lane 4 vs 3 in Fig. 5H). We performed immunofluorescence staining to confirm that ITPR3 is necessary for statin-activated eNOS. The co-localization of eNOS with Cav-1 at the basal level, presumably in lipid rafts, is disrupted by atorvastatin treatment (Fig. 5I).

KLF4 regulates the *ITPR3* chromatin accessibility

In the promoter region of *ITPR3*, we identified 6 putative KLF4 binding sites (shown in Sup. Table 1). DNA segments flanking these KLF4 cognate binding sequence showed enriched H3K27ac signals and increased chromatin accessibility, as revealed by ChIP-seq and ATAC-seq, respectively (Fig. 6A). By using KLF4 ChIP-qPCR, we verified that KLF4

overexpression increased KLF4 binding to all these 6 KLF4 binding sites (Fig. 6B). However, H3K27ac ChIP-PCR revealed the greatest enrichment of H3K27ac near the 1st and 5th sites (Fig. 6C).

To further test whether KLF4 binding to its cognate binding sequence affects histone H3K27ac modification, we deleted the 1st KLF4 binding site in the *ITPR3* promoter in ECs ($ITPR3^{\Delta BS}$) by using CRISPR-Cas9 genomic editing (Fig. 7A). Deletion of this binding site indeed decreased KLF4 binding, with concurrent attenuations of H3K27ac modification, chromatin accessibility, Pol II recruitment, and ITPR3 mRNA expression (Fig. 7B and 7C). These data suggest that KLF4, acting as a PS-inducible pioneer TF, regulates ITPR3 expression by remodeling histone and the consequent chromatin accessibility of the *ITPR3* promoter. Functionally, the ionomycin-induced calcium influx was significantly lower in $ITPR3^{\Delta BS}$ than wild-type ECs (Fig. 7D). Furthermore, the dissociation of eNOS-Cav-1 and association of eNOS-calmodulin seen in wild-type ECs stimulated with atorvastatin or PS were largely abolished in $ITPR3^{\Delta BS}$ ECs (Fig. 7E, 7F). Thus, the physiological (i.e., PS) and pharmacological (i.e., statins) stimulations of eNOS-derived NO bioavailability are contributed, at least in part, by KLF4 regulation of ITPR3 via chromatin remodeling.

Discussion

Vascular tone is regulated by EC responses to mechanical and biochemical stimuli, and $[Ca^{2+}]_i$-modulated eNOS activity plays a significant role in this regulation. By using NGS, including RNA-seq, ChIP-seq, and ATAC-seq, we have found that KLF4, functioning as a PS-induced pioneer TF, activates ITPR3 via epigenetic regulation. This finding indicates that PS and statins augment the eNOS-derived NO bioavailability, at least in part, via KLF4-induced ITPR3.

$[Ca^{2+}]_i$ in ECs can be regulated by voltage-dependent calcium channels, Ca^{2+}-induced calcium release from ryanodine receptors, and Ca^{2+} release from ITPR stores. There is substantial evidence that the increase in $[Ca^{2+}]_i$ with the ensuing activation of the IP3-ITPR pathway leads to an increase in the production of NO and other vasodilatory factors[21,22]. In a recent study by Yuan *et al.*, mice with endothelial deletion of *Itpr1* showed reduced eNOS activity, blunted vasodilation, and elevated blood pressure[22]. Our current study suggested a mechanism by which the PS-induced KLF4 increased its binding to the promoter region of *ITPR3* in a *trans* manner, altered chromatin accessibility in a *cis* manner (as revealed by enrichment of H3K27ac and ATAC-seq), and then recruited Pol II to transactivate ITPR3.

Three ITPR subtypes have been reported: ITPR1, ITPR2, and ITPR3[47]. Our RNA-seq data indicate that ITPR3 is the major type in cultured ECs (Sup. Fig. 3). Furthermore, the upstream promoter region of *ITPR3* seems to have more putative KLF4 binding sites and PS-enriched H3K27ac signals than *ITPR1*and *ITPR2* (Sup. Fig. 4). Functionally, the KLF4-transactivated ITPR3 regulates the IP3-ITPR pathway both at the basal level and under PS. These two modes of regulation would constitute lineage- and signal-dependent ITPR3 transcription, respectively, to provide the basal and stimulatory regulation of $[Ca^{2+}]_i$ signaling essential for maintaining vascular tone.

The selection of the 18 PS-induced genes for further validation was based on the results of KLF4 binding, histone remodeling by ChIP-seq, and expression levels by RNA-seq. As one of the four Yamanaka factors, KLF4 binds to the target DNA sequence via its zinc-finger domain, which enhances transcription by recruiting transcription machinery and Pol II[48]. Acting as a master TF in ECs[49], KLF4 not only is important for the endothelial lineage but also activates genes essential for EC homeostasis [e.g., eNOS and cholesterol-25-hydroxylase][34,50]. Functionally, KLF4 is upregulated by atheroprotective flow and cholesterol-lowering drugs (e.g., statins)[4,40]. Mechanistically, KLF4 binds to Sp1-like binding sites on the promoter regions of KLF4-targeted genes[51]. Furthermore, KLF4 interacts with histone acetyltransferases or deacetylases to increase or attenuate chromatin acetylation, respectively, thereby affecting transcription. For example, KLF4 can regulate chromatin remodeling of interleukin 6 promoter in dendritic cells by changing the adjunct histone modification[52]. In normal breast epithelial cells, KLF4 recruitment of HDAC2/3 to the vascular endothelial growth factor (*VEGF*) promoter represses the expression of VEGF[53]. KLF4-driven histone modification in transactivating *ITPR3* was further supported by the decondensed chromatin in *loci* adjacent to the KLF4 binding sites. In the context of PS induction of ITPR3 in ECs, Pol II is recruited to the KLF4-occupied *ITPR3* promoter for transcriptional initiation (Fig. 7C).

Although we focused on KLF4 as the key TF, KLF4 and KLF2 bind to similar *cis*-elements (e.g., Sp1-like binding site) to transactivate commonly targeted genes such as eNOS and thrombomodulin (THBD)[49]. Atheroprotective flow and pharmacological agents such as statins induce optimal levels of KLF2 and/or KLF4 to maintain EC homeostasis[4,40,54,55]. While KLF2 and KLF4 seem to be compensatory for each other in maintaining EC function via the commonly transactivated genes, ablations of both lead to EC dysfunction more than either alone[16]. Thus, KLF2 and KLF4 likely synergize each other to orchestrate the transcriptional machinery in regulating genes such as NOS3, THBD, and ITPR3. The detailed mechanism underlying this synergism deserves further investigation by including KLF2 ChIP-seq and ATAC-seq analyses in addition to KLF4.

Approximately 85% of the coding regions in the human and mouse genome are similar, but conservation between the non-coding regions of human and mouse genomes is moderate[56]. Nevertheless, mouse models with EC-specific overexpression of *klf4* decreases atherosclerosis in atheroprone areas, whereas EC-specific ablation of *klf4* increases atherosclerosis in atheroprotective areas[34]. Indeed, opposite trends of KLF4 and ITPR3 expression are evident in mouse AA vs. TA areas (Fig. 4A). These opposing transcriptional and phenotypic outcomes demonstrate the importance of flow regulation of KLF4 in the mouse vasculature. We found five putative KLF4 binding sites predicted in the promoter region of the mouse *Itpr3* gene (Sup. Fig. 5), which suggests that mouse *Itpr3* may also undergo chromatin remodeling initiated by KLF4 binding. Data in Fig. 5B show that KLF4 binding to site 1 at −1207 and site 5 at −10318 of the *ITPR3* promoter caused chromatin remodeling to a reduced compact state, as shown by H3K27ac enrichment and ATAC-seq peaks. Interestingly, deletion of site 1 affected KLF4 binding and chromatin remodeling at site 5 (Sup. Fig. 6). Hence, these two KLF4 binding sites, separated by ~9 kb, may crosstalk to co-regulate the expression of ITPR3.

In summary, using a multi-layer and genome-wide approach, we have made the novel discovery that the PS-induced KLF4 regulates the transcriptome in ECs epigenetically and transcriptionally. Furthermore, we have demonstrated that ITPR3 plays a critical role as a KLF4-regulated gene in mediating H3K27ac enrichment and chromatin accessibility, and hence Ca^{2+}-dependent eNOS activation and EC homeostasis.

Supplementary Material

Refer to Web version on PubMed Central for supplementary material.

Acknowledgments

The authors thank Drs. Brendan Gongol, Traci Marin, Nathan Spann, Phu Nguyen, Julie Yi-Shuan Li, Mano R. Maurya, and Shankar Subramaniam at University of California, San Diego, and Chun-San Tai at National Chiao Tung University for technical assistance, useful discussions, and their valuable suggestions, and Drs. Mukesh Jian, Panjamaporn Sangwung, and Guangjin Zhou, School of Medicine, Case Western University, for providing lung ECs from EC-KLF4-Tg and EC-KLF4$^{-/-}$ mice.

Sources of Funding

This work was supported in part by NIH research grants R01HL108735 (to J.Y-J.S. and S.C.), R01HL125643 (to J.Y-J.S.), R01GM111665 (to Jin Zhang), K99/R00HL122368 (to Z.C.), 5T32HL007444 (to M.M.), American Heart Association Postdoctoral Fellowship 17POST33410101 (to T.-S.H.), Taiwan Ministry of Science and Technology grants MOST 106–2917-I-009–016 (to H.-D.H.), MOST 107–2633-B-009–003 (to H.-D.H., W.-T.W.).

Abbreviations

AA	aortic arch
ATAC-seq	assay for transposase-accessible chromatin-sequencing
Cav-1	Caveolin-1
ChIP-Seq	chromatin immunoprecipitation followed by high throughput sequencing
EC	endothelial cell
eNOS	Endothelial nitric oxide synthase
HUVECs	human umbilical vein endothelial cells
H3K4me1	mono-methylation of histone 3 lysine 4
H3K27ac	acetylation of histone 3 lysine 27
ITPR3	Inositol 1,4,5-trisphosphate receptor 3
KLF4	Krüppel-like factor 4
NGS	next-generation sequencing
NO	nitric oxide
OS	oscillatory shear stress

Pol II	RNA polymerase II
PS	pulsatile shear stress
TA	thoracic aorta
TF	transcription factors
THBD	Thrombomodulin
VEGF	Vascular endothelial growth factor

References

1. Chiu JJ, Chien S. Effects of disturbed flow on vascular endothelium: Pathophysiological basis and clinical perspectives. Physiol. Rev 2011;91:327–387. [PubMed: 21248169]
2. Gimbrone MA Jr., Garcia-Cardena G Endothelial cell dysfunction and the pathobiology of atherosclerosis. Circ. Res 2016;118:620–636. [PubMed: 26892962]
3. Baeyens N, Bandyopadhyay C, Coon BG, Yun S, Schwartz MA. Endothelial fluid shear stress sensing in vascular health and disease. J. Clin. Invest 2016;126:821–828. [PubMed: 26928035]
4. McCormick SM, Eskin SG, McIntire LV, Teng CL, Lu CM, Russell CG, Chittur KK. DNA microarray reveals changes in gene expression of shear stressed human umbilical vein endothelial cells. Proc. Natl. Acad. Sci. U. S. A 2001;98:8955–8960. [PubMed: 11481467]
5. Chen BP, Li YS, Zhao Y, Chen KD, Li S, Lao J, Yuan S, Shyy JY, Chien S. DNA microarray analysis of gene expression in endothelial cells in response to 24-h shear stress. Physiol. Genomics 2001;7:55–63. [PubMed: 11595792]
6. Ajami NE, Gupta S, Maurya MR, Nguyen P, Li JY, Shyy JY, Chen Z, Chien S, Subramaniam S. Systems biology analysis of longitudinal functional response of endothelial cells to shear stress. Proc. Natl. Acad. Sci. U. S. A 2017;114:10990–10995. [PubMed: 28973892]
7. Zhou J, Li YS, Chien S. Shear stress-initiated signaling and its regulation of endothelial function. Arterioscler. Thromb. Vasc. Biol 2014;34:2191–2198. [PubMed: 24876354]
8. Lee DY, Lee CI, Lin TE, Lim SH, Zhou J, Tseng YC, Chien S, Chiu JJ. Role of histone deacetylases in transcription factor regulation and cell cycle modulation in endothelial cells in response to disturbed flow. Proc. Natl. Acad. Sci. U. S. A 2012;109:1967–1972. [PubMed: 22308472]
9. Jiang YZ, Jimenez JM, Ou K, McCormick ME, Zhang LD, Davies PF. Hemodynamic disturbed flow induces differential DNA methylation of endothelial kruppel-like factor 4 promoter in vitro and in vivo. Circ. Res 2014;115:32–43. [PubMed: 24755985]
10. Dunn J, Qiu H, Kim S, Jjingo D, Hoffman R, Kim CW, Jang I, Son DJ, Kim D, Pan C, Fan Y, Jordan IK, Jo H. Flow-dependent epigenetic DNA methylation regulates endothelial gene expression and atherosclerosis. J. Clin. Invest 2014;124:3187–3199. [PubMed: 24865430]
11. Huang TS, Wang KC, Quon S, Nguyen P, Chang TY, Chen Z, Li YS, Subramaniam S, Shyy J, Chien S. Linc00341 exerts an anti-inflammatory effect on endothelial cells by repressing vcam1. Physiol. Genomics 2017;49:339–345. [PubMed: 28500253]
12. Miao Y, Ajami NE, Huang TS, Lin FM, Lou CH, Wang YT, Li S, Kang J, Munkacsi H, Maurya MR, Gupta S, Chien S, Subramaniam S, Chen Z. Enhancer-associated long non-coding rna leene regulates endothelial nitric oxide synthase and endothelial function. Nat Commun. 2018;9:292. [PubMed: 29348663]
13. Heintzman ND, Hon GC, Hawkins RD, et al. Histone modifications at human enhancers reflect global cell-type-specific gene expression. Nature. 2009;459:108–112. [PubMed: 19295514]
14. Whyte WA, Orlando DA, Hnisz D, Abraham BJ, Lin CY, Kagey MH, Rahl PB, Lee TI, Young RA. Master transcription factors and mediator establish super-enhancers at key cell identity genes. Cell. 2013;153:307–319. [PubMed: 23582322]
15. Donaghey J, Thakurela S, Charlton J, et al. Genetic determinants and epigenetic effects of pioneer-factor occupancy. Nat. Genet 2018;50:250–258. [PubMed: 29358654]

16. Ren B, Robert F, Wyrick JJ, Aparicio O, Jennings EG, Simon I, Zeitlinger J, Schreiber J, Hannett N, Kanin E, Volkert TL, Wilson CJ, Bell SP, Young RA. Genome-wide location and function of DNA binding proteins. Sci. 2000;290:2306–2309.
17. Buenrostro JD, Giresi PG, Zaba LC, Chang HY, Greenleaf WJ. Transposition of native chromatin for fast and sensitive epigenomic profiling of open chromatin, DNA-binding proteins and nucleosome position. Nat. Methods 2013;10:1213–1218. [PubMed: 24097267]
18. Creyghton MP, Cheng AW, Welstead GG, Kooistra T, Carey BW, Steine EJ, Hanna J, Lodato MA, Frampton GM, Sharp PA, Boyer LA, Young RA, Jaenisch R. Histone h3k27ac separates active from poised enhancers and predicts developmental state. Proc. Natl. Acad. Sci. U. S. A 2010;107:21931–21936. [PubMed: 21106759]
19. Ernst J, Kheradpour P, Mikkelsen TS, Shoresh N, Ward LD, Epstein CB, Zhang X, Wang L, Issner R, Coyne M, Ku M, Durham T, Kellis M, Bernstein BE. Mapping and analysis of chromatin state dynamics in nine human cell types. Nature. 2011;473:43–49. [PubMed: 21441907]
20. Santulli G, Nakashima R, Yuan Q, Marks AR. Intracellular calcium release channels: An update. J. Physiol 2017;595:3041–3051. [PubMed: 28303572]
21. Singleton PA, Bourguignon LY. Cd44 interaction with ankyrin and ip3 receptor in lipid rafts promotes hyaluronan-mediated ca2+ signaling leading to nitric oxide production and endothelial cell adhesion and proliferation. Exp. Cell Res 2004;295:102–118. [PubMed: 15051494]
22. Yuan Q, Yang J, Santulli G, Reiken SR, Wronska A, Kim MM, Osborne BW, Lacampagne A, Yin Y, Marks AR. Maintenance of normal blood pressure is dependent on ip3r1-mediated regulation of enos. Proc. Natl. Acad. Sci. U. S. A 2016;113:8532–8537. [PubMed: 27402766]
23. Wu S, Lu Q, Wang Q, Ding Y, Ma Z, Mao X, Huang K, Xie Z, Zou MH. Binding of fun14 domain containing 1 with inositol 1,4,5-trisphosphate receptor in mitochondria-associated endoplasmic reticulum membranes maintains mitochondrial dynamics and function in hearts in vivo. Circulation. 2017;136:2248–2266. [PubMed: 28942427]
24. Thul PJ, Akesson L, Wiking M, et al. A subcellular map of the human proteome. Sci. 2017;356.
25. Xiao H, Lu M, Lin TY, et al. Sterol regulatory element binding protein 2 activation of nlrp3 inflammasome in endothelium mediates hemodynamic-induced atherosclerosis susceptibility. Circulation. 2013;128:632–642. [PubMed: 23838163]
26. Bolger AM, Lohse M, Usadel B. Trimmomatic: A flexible trimmer for illumina sequence data. Bioinformatics. 2014;30:2114–2120. [PubMed: 24695404]
27. Kim D, Langmead B, Salzberg SL. Hisat: A fast spliced aligner with low memory requirements. Nat. Methods 2015;12:357–360. [PubMed: 25751142]
28. Liao Y, Smyth GK, Shi W. Featurecounts: An efficient general purpose program for assigning sequence reads to genomic features. Bioinformatics. 2014;30:923–930. [PubMed: 24227677]
29. Love MI, Huber W, Anders S. Moderated estimation of fold change and dispersion for rna-seq data with deseq2. Genome Biol. 2014;15:550. [PubMed: 25516281]
30. Langmead B, Salzberg SL. Fast gapped-read alignment with bowtie 2. Nat. Methods 2012;9:357–359. [PubMed: 22388286]
31. Heinz S, Benner C, Spann N, Bertolino E, Lin YC, Laslo P, Cheng JX, Murre C, Singh H, Glass CK. Simple combinations of lineage-determining transcription factors prime cis-regulatory elements required for macrophage and b cell identities. Mol. Cell 2010;38:576–589. [PubMed: 20513432]
32. Ramirez F, Ryan DP, Gruning B, Bhardwaj V, Kilpert F, Richter AS, Heyne S, Dundar F, Manke T. Deeptools2: A next generation web server for deep-sequencing data analysis. Nucleic Acids Res. 2016;44:W160–165. [PubMed: 27079975]
33. Nguyen NTT, Contreras-Moreira B, Castro-Mondragon JA, Santana-Garcia W, Ossio R, Robles-Espinoza CD, Bahin M, Collombet S, Vincens P, Thieffry D, van Helden J, Medina-Rivera A, Thomas-Chollier M. Rsat 2018: Regulatory sequence analysis tools 20th anniversary. Nucleic Acids Res. 2018;46:W209–W214. [PubMed: 29722874]
34. Zhou G, Hamik A, Nayak L, et al. Endothelial kruppel-like factor 4 protects against atherothrombosis in mice. J. Clin. Invest 2012;122:4727–4731. [PubMed: 23160196]
35. Chari R, Yeo NC, Chavez A, Church GM. Sgrna scorer 2.0: A species-independent model to predict crispr/cas9 activity. ACS Synth Biol. 2017;6:902–904. [PubMed: 28146356]

36. Sanjana NE, Shalem O, Zhang F. Improved vectors and genome-wide libraries for crispr screening. Nat. Methods 2014;11:783–784. [PubMed: 25075903]
37. Kilpinen H, Waszak SM, Gschwind AR, et al. Coordinated effects of sequence variation on DNA binding, chromatin structure, and transcription. Sci. 2013;342:744–747.
38. ENCODE Project Consortium. An integrated encyclopedia of DNA elements in the human genome. Nature. 2012;489:57–74. [PubMed: 22955616]
39. Hu C, Liu M, Zhang W, Xu Q, Ma K, Chen L, Wang Z, He S, Zhu H, Xu N. Upregulation of klf4 by methylseleninic acid in human esophageal squamous cell carcinoma cells: Modification of histone h3 acetylation through hat/hdac interplay. Mol. Carcinog 2015;54:1051–1059. [PubMed: 24789055]
40. Maejima T, Inoue T, Kanki Y, et al. Direct evidence for pitavastatin induced chromatin structure change in the klf4 gene in endothelial cells. PLoS One. 2014;9:e96005. [PubMed: 24797675]
41. Fulton D, Gratton JP, McCabe TJ, Fontana J, Fujio Y, Walsh K, Franke TF, Papapetropoulos A, Sessa WC. Regulation of endothelium-derived nitric oxide production by the protein kinase akt. Nature. 1999;399:597–601. [PubMed: 10376602]
42. Dimmeler S, Fleming I, Fisslthaler B, Hermann C, Busse R, Zeiher AM. Activation of nitric oxide synthase in endothelial cells by akt-dependent phosphorylation. Nature. 1999;399:601–605. [PubMed: 10376603]
43. Fleming I, Fisslthaler B, Dimmeler S, Kemp BE, Busse R. Phosphorylation of thr(495) regulates ca(2+)/calmodulin-dependent endothelial nitric oxide synthase activity. Circ. Res 2001;88:E68–75. [PubMed: 11397791]
44. Foskett JK, White C, Cheung KH, Mak DO. Inositol trisphosphate receptor ca2+ release channels. Physiol. Rev 2007;87:593–658. [PubMed: 17429043]
45. Boo YC, Kim HJ, Song H, Fulton D, Sessa W, Jo H. Coordinated regulation of endothelial nitric oxide synthase activity by phosphorylation and subcellular localization. Free Radic. Biol. Med 2006;41:144–153. [PubMed: 16781462]
46. Michel JB, Feron O, Sacks D, Michel T. Reciprocal regulation of endothelial nitric-oxide synthase by ca2+-calmodulin and caveolin. J. Biol. Chem 1997;272:15583–15586. [PubMed: 9188442]
47. Taylor CW, Genazzani AA, Morris SA. Expression of inositol trisphosphate receptors. Cell Calcium. 1999;26:237–251. [PubMed: 10668562]
48. Liu L, Xu Y, He M, et al. Transcriptional pause release is a rate-limiting step for somatic cell reprogramming. Cell Stem Cell. 2014;15:574–588. [PubMed: 25312495]
49. Sangwung P, Zhou G, Nayak L, et al. Klf2 and klf4 control endothelial identity and vascular integrity. JCI Insight. 2017;2:e91700. [PubMed: 28239661]
50. Li Z, Martin M, Zhang J, et al. Kruppel-like factor 4 regulation of cholesterol-25-hydroxylase and liver x receptor mitigates atherosclerosis susceptibility. Circulation. 2017;136:1315–1330. [PubMed: 28794002]
51. Kaczynski J, Cook T, Urrutia R. Sp1- and kruppel-like transcription factors. Genome Biol. 2003;4:206. [PubMed: 12620113]
52. Rosenzweig JM, Glenn JD, Calabresi PA, Whartenby KA. Klf4 modulates expression of il-6 in dendritic cells via both promoter activation and epigenetic modification. J. Biol. Chem 2013;288:23868–23874. [PubMed: 23846700]
53. Ray A, Alalem M, Ray BK. Loss of epigenetic kruppel-like factor 4 histone deacetylase (klf-4-hdac)-mediated transcriptional suppression is crucial in increasing vascular endothelial growth factor (vegf) expression in breast cancer. J. Biol. Chem 2013;288:27232–27242. [PubMed: 23926105]
54. Dekker RJ, van Soest S, Fontijn RD, Salamanca S, de Groot PG, VanBavel E, Pannekoek H, Horrevoets AJ. Prolonged fluid shear stress induces a distinct set of endothelial cell genes, most specifically lung kruppel-like factor (klf2). Blood. 2002;100:1689–1698. [PubMed: 12176889]
55. Parmar KM, Nambudiri V, Dai G, Larman HB, Gimbrone MA Jr., Garcia-Cardena G Statins exert endothelial atheroprotective effects via the klf2 transcription factor. J. Biol. Chem 2005;280:26714–26719. [PubMed: 15878865]

56. Dietrich WF, Miller J, Steen R, Merchant MA, Damron-Boles D, Husain Z, Dredge R, Daly MJ, Ingalls KA, O'Connor TJ. A comprehensive genetic map of the mouse genome. Nature. 1996;380:149–152. [PubMed: 8600386]

Highlights

- By using RNA-seq, ChIP-seq, and ATAC-seq, we found that KLF4, functioning as a PS-induced transcription factor in ECs, activates ITPR3 transcriptionally and epigenetically.
- KLF4 regulates ITPR3 expression by mediating H3K27ac enrichment and chromatin accessibility in the promoter region.
- PS induction of ITPR3 augments Ca^{2+}-dependent eNOS activation and EC homeostasis.
- PS and statins increase the eNOS-derived NO bioavailability, at least in part, by KLF4-induction of ITPR3.
- This innovative systemic approach identifies many other PS-inducible molecules and pathways through the similar mechanism.

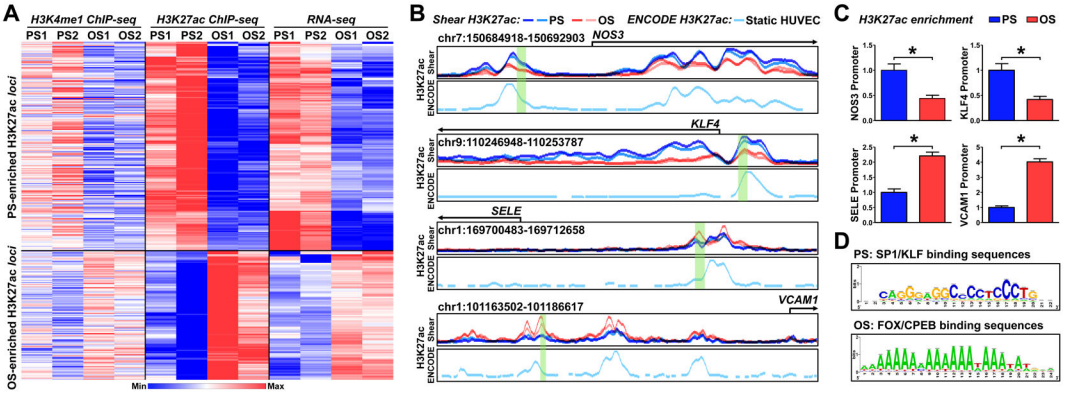

Figure 1. Shear stress regulation of histone modifications, assessed by H3K4me1 ChIP-seq, H3K27ac ChIP-seq, and RNA-seq.

(A, B) Human umbilical vein endothelial cells (HUVECs) were exposed to pulsatile flow (PS; 12 ± 4 dyn/cm^2) or oscillatory flow (OS; 1 ± 4 dyn/cm^2) for 16 hr. Cells from two biological repeats (PS1, OS1, PS2, OS2) were subjected to H3K4me1 ChIP-seq, and H3K27ac ChIP-seq, and RNA-seq analyses. (**A**) Heat map of the normalized H3K4me1 and H3K27ac enrichment and RNA-seq signal of the nearest expressed genes. The genes represented were those with H3K27ac and mRNA enrichment by PS. (**B**) Normalized PS (blue)- or OS (red)-associated H3K27ac ChIP signals at the promoter regions of *NOS3*, *KLF4*, *SELE*, and *VCAM1*. The H3K27ac enrichment in static HUVECs (light turquoise, below the PS and OS H3K27ac) were adopted from ENCODE (GSM733691)[38]. (**C**) HUVECs were exposed to PS or OS. H3K27ac enrichment in the region highlighted in green (in B) was evaluated by H3K27ac ChIP-qPCR. Data are mean ± SEM from 3 independent experiments. Statistical significance was determined by 2-tailed Mann-Whitney U test between PS and OS. *$P < 0.05$. (**D**) PS- or OS-enhanced H3K27ac hyper-condensed regions were analyzed by RSAT to decipher TF binding sites.

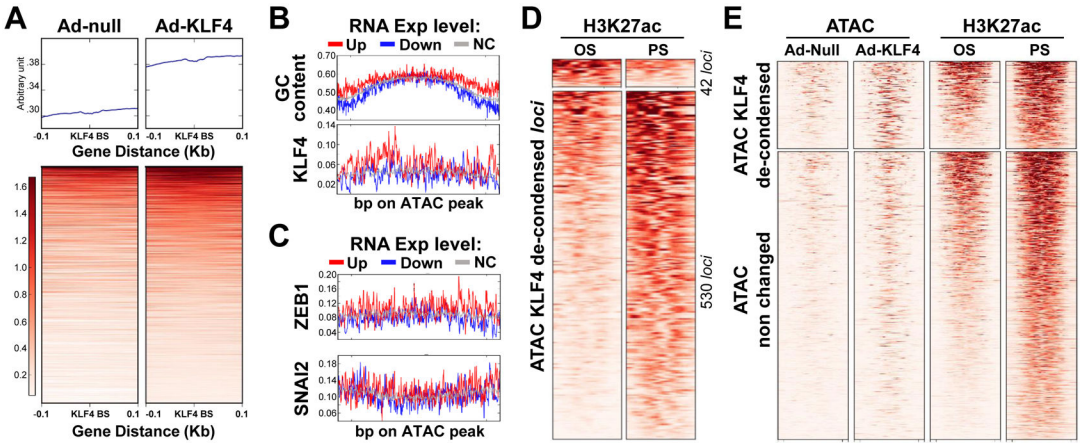

Figure 2. KLF4 regulation of PS-induced genes via chromatin remodeling, assessed by ATAC-seq.

HUVECs were transfected with Ad-null or Ad-KLF4 for 24 hr. Cells were subjected to ATAC-seq. (**A**) ATAC peaks from Ad-null or Ad-KLF4-infected ECs were initially merged into a union set of ATAC peaks. The KLF4 putative binding sites within the ATAC peaks were then predicted. The upper and lower panels show the overall and per-*loci* ATAC signals at ± 0.1 kb flanking the putative KLF4 binding sites. (**B, C**) ATAC *loci* were first divided into 3 groups by the expression levels of their closest genes induced by PS. The assessed GC ratio or frequency of putative TF binding in these *loci* are summarized in the representative heat maps. The x-axis represents the position of the de-condensed *loci* and the y-axis the frequency of changes. (**D**) Heat maps showing 572 *loci* de-condensed by KLF4, as assessed by ATAC-seq. These *loci* coincide with the PS- or OS-associated H3K27ac enrichment. (**E**) Heat maps of the ATAC-seq and H3K27ac ChIP-seq signals in *loci* de-condensed or not by KLF4. Distance at the abscissa denotes the relative location within the *loci*, and each row represents a *locus*.

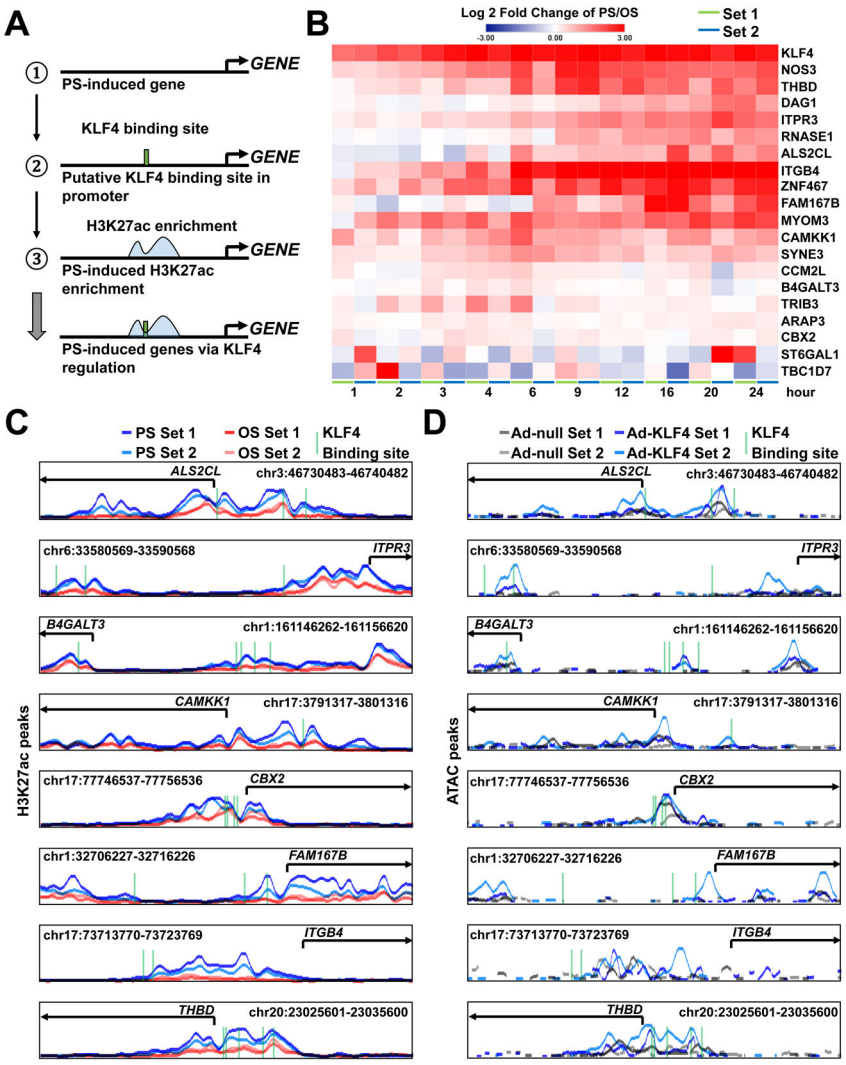

Figure 3. PS-induced genes via KLF4-dependent chromatin remodeling.

(**A**) Three selective criteria for the PS-induced genes (see text). (**B**) Heat map indicating differentially expressed mRNAs for the 18 selected genes. The presented data were selected from the 10-time point RNA-seq reported by Ajami *et. al*[6]. (**C**) Normalized PS (blue)- or OS (red)-induced H3K27ac enrichment in the promoter regions of *ALS2CL*, *ITPR3*, *B4GALT3*, *CAMKK1*, *CBX2*, *FAM167B*, *ITGB4*, and *THBD*. The putative KLF4 binding sites in the respective promoter regions are illustrated in green. (**D**) HUVECs were infected with Ad-null or Ad-KLF4 for 24 hr in two biological repeats. ATAC-seq was performed to evaluate the chromatin accessibility. Lines in gray (from Ad-null–infected ECs) and blue (from Ad-KLF4–infected ECs) represent ATAC signals in the same *loci* as those in (C).

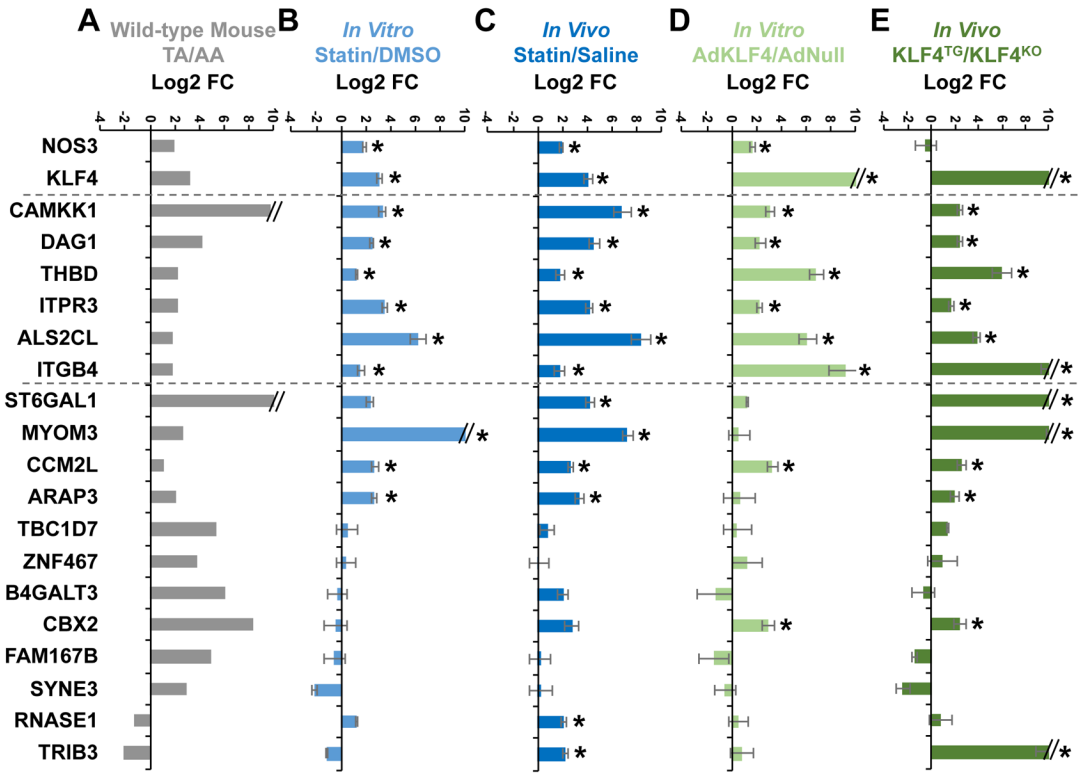

Figure 4. KLF4-dependent gene expression in ECs.

(**A**) Intima isolated from thoracic aorta (TA) and aortic arch (AA) of five C57BL/6j mice (3 male and 2 female) were pooled. (**B**) HUVECs were treated with atorvastatin (5 μM) or DMSO for 24 hr. (**C**) C57BL/6j mice were intraperitoneally injected with atorvastatin (50 mg/kg) or an equal volume of saline (500 μL) randomly. Lung ECs were harvested 24 hr post-injection, n=6 mice (3 male and 3 female) in each group. (**D**) HUVECs were infected with Ad-null or Ad-KLF4 for 24 hr. (**E**) Lung ECs were isolated from EC-KLF4$^{-/-}$ or EC-KLF4-Tg mice, n=3 mice in each group. The expression of the identified 18 genes (shown in Fig. 3 and Table 1) was detected by RT-qPCR and presented by Log 2 fold change (Log 2 FC). Data are mean ± SEM from 3 independent experiments for (B) and (D). Statistical significance was determined by 2-tailed Mann-Whitney U test. *$P < 0.05$ compared with control.

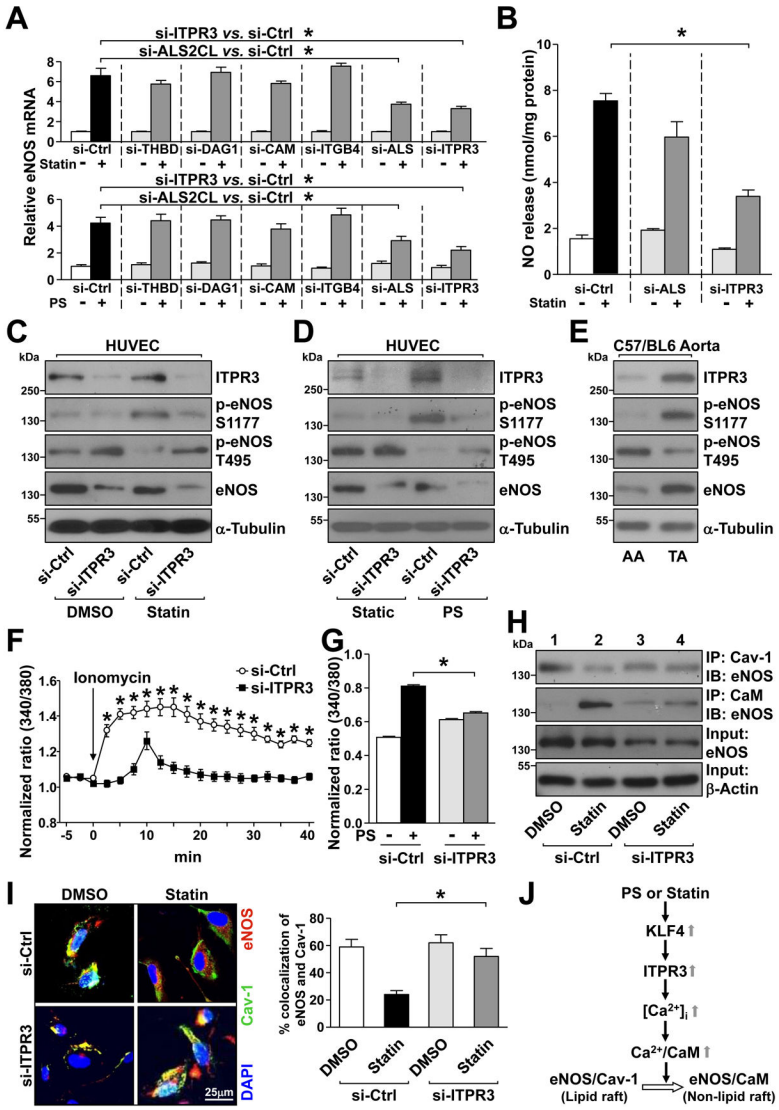

Figure 5. Atorvastatin and PS upregulate the ITPR3-eNOS axis in ECs.

(**A)** HUVECs were transfected with siRNA against THBD, DAG1, CAMKK1, ITGB4, ALS2CL, or ITPR3 for 48 hr. In control experiments, HUVECs were transfected with control siRNA. After atorvastatin (5 μM) or PS stimulation for the last 16 hr, cells were lysed and eNOS mRNA level was detected by RT-qPCR. (**B**) HUVECs were transfected with ALS2CL siRNA, ITPR3 siRNA, or control siRNA. After atorvastatin stimulation for 1 hr, NO level was detected by Griess reagent. (**C, D, F, G, H, I**) HUVECs were transfected with ITPR3 siRNA or control siRNA, and then stimulated with atorvastatin (C, H, I) for 1 hr, PS for 1 hr (D), or PS for 10 mins (G). (**E**) Tissues isolated from TA and AA of C57BL/6j mice (pooled from 3 male and 2 female mice). In (C-E), the cellular or tissue extracts were examined by western blot analysis for protein levels of ITPR3, p-eNOS T495, p-eNOS S1177, eNOS, and α-tubulin. In (**F, G**), ECs were treated with Fura2-AM for 1 hr before stimulation with ionomycin (2 μM, F) or PS (G). The calcium influx rate was detected by comparing the 340/380-nm ratio under a fluorescence microscope. Overall, 12–15 cells (F)

or 130–160 cells (G) were randomly chosen to detect the fluorescence in each group. In (**H**), cell lysates were immunoprecipitated (IP) with anti-Cav-1 or anti-calmodulin (CaM) antibody. The co-immunoprecipitated eNOS was evaluated by immunoblotting (IB), with β-actin as a loading control. In (**I**), immunostaining was performed with anti-eNOS (red) or anti-Cav-1 (green) antibody. Nuclei were counterstained with DAPI (blue). Fluorescence was detected under an Olympus confocal microscope. The colocalization of eNOS and caveolin-1 was quantified by ImageJ. (**J**) A working model of atorvastatin and PS regulation of the ITPR3-eNOS axis via KLF4. Data are mean ± SEM from at least 3 independent experiments. For parametric data (F, G, I), statistical significance was determined by 2-tailed Student's *t* test between two indicated groups. Non parametric data (A, B) were analyzed using Kruskal-Wallis with Dunn's post-hoc test. $*P < 0.05$.

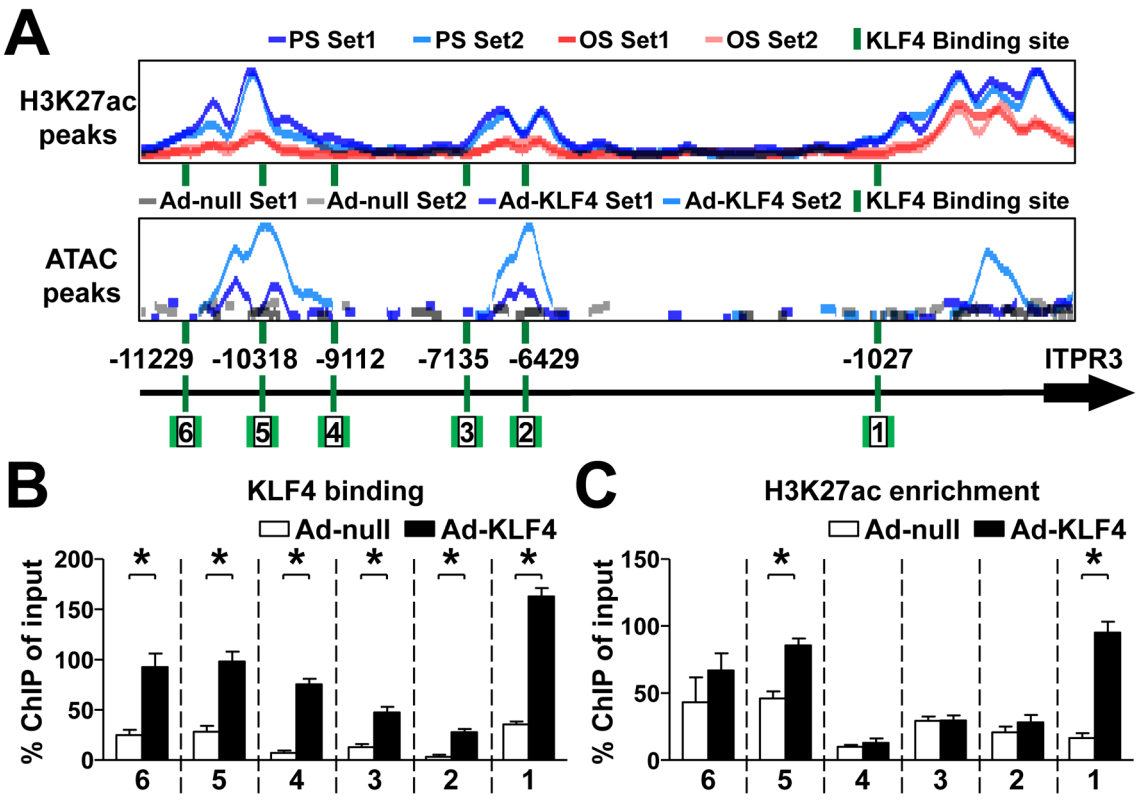

Figure 6. KLF4 regulates ITPR3 by modulating chromatin accessibility.

(**A**) Putative KLF4 binding sites, PS- or OS-induced H3K27ac enrichment, and Ad-null- or Ad-KLF4-induced ATAC signals in the *ITPR3* promoter. (**B, C**) HUVECs were infected with Ad-null or Ad-KLF4 for 24 hr. KLF4 binding to the *ITPR3* promoter and H3K27ac enrichment of the *ITPR3* promoter were detected by KLF4 ChIP-qPCR and H3K27ac ChIP-qPCR, respectively. The used PCR primers were depicted by arrows in Panel A. Data are mean ± SEM from at least 3 independent experiments. Statistical significance was determined by 2-tailed Mann-Whitney U test between two indicated groups. **P* < 0.05.

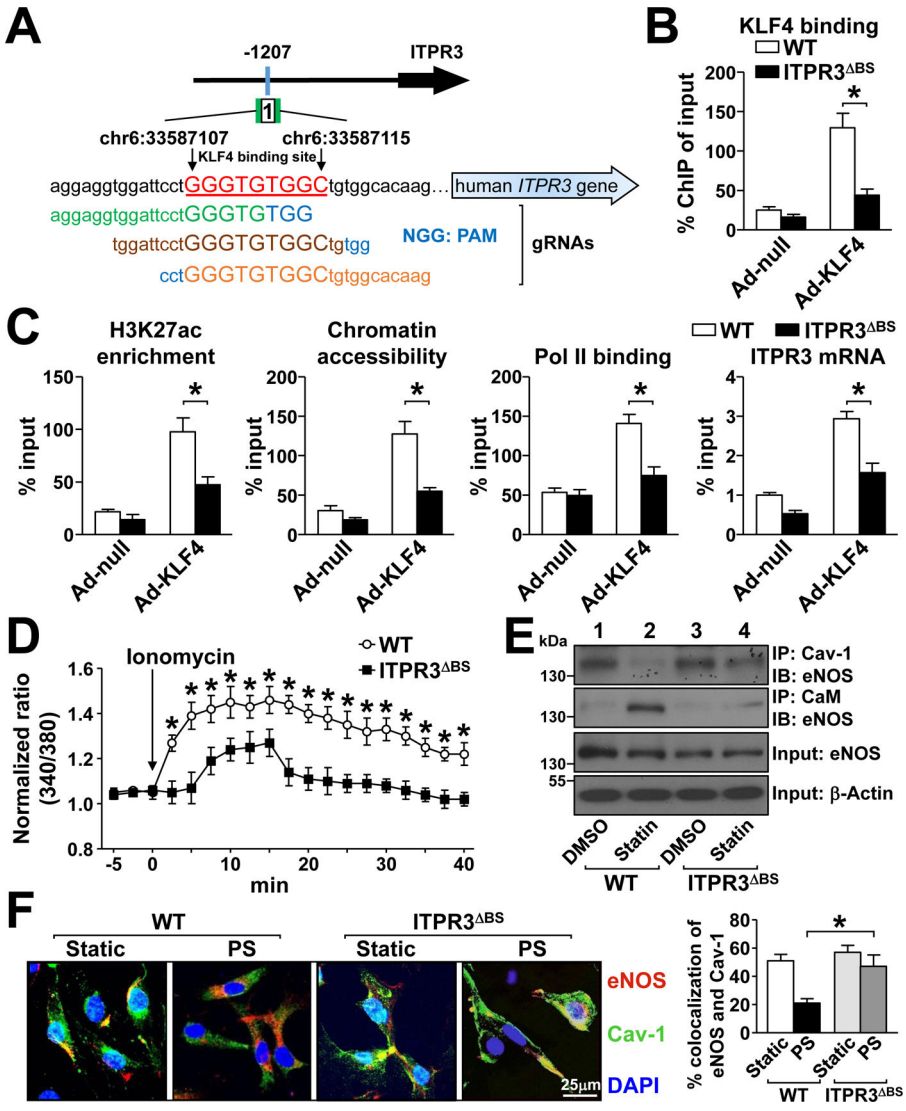

Figure 7. KLF4-dependent activation of the ITPR3-eNOS axis.

(**A**) CRISPR-Cas9 strategy for targeting the 1st KLF4 binding site (chr6:33587106-chr6:33587115) in the *ITPR3* promoter. (**B, C**) Wild-type HUVECs or CRISPR-Cas9-edited HUVECs (ITPR3$^{\Delta BS}$) were infected with Ad-null or Ad-KLF4. KLF4 binding, H3K27ac enrichment, and chromatin accessibility near the KLF4 binding site 1 were detected by KLF4-ChIP, H3K27ac-ChIP, and ATAC-qPCR, respectively. Pol II recruitment near the TSS site was detected by Pol II-ChIP-qPCR, and the ITPR3 mRNA level was assayed by qPCR. (**D, E, F**) Wild-type and ITPR3$^{\Delta BS}$ HUVECs were stimulated with ionomycin, atorvastatin, or PS. The calcium influx rate (D), Cav-1-eNOS or CaM-eNOS co-immunoprecipitation (E), and immunostaining (F) were as described in Figure 5. Data are mean ± SEM from at least 3 independent experiments. For parametric data (D, F), statistical significance was determined by 2-tailed Student's *t* test between two indicated groups. Non parametric data (B, C) were analyzed using 2-tailed Mann-Whitney U test between 2 indicated groups. **P* < 0.05.

Table 1,

Characteristics of 18 PS-induced genes

Symbol	Aliases	Full name	Location	Gene ID
ITGB4	CD104; GP150	Integrin subunit beta 4	17q25.1	3691
ZNF467	EZI; Zfp467	Zinc finger protein 467	7q36.1	168544
ST6GALNAC1	STYI; SIAT7A; ST6GalNAcI	ST6 N-acetylgalactosaminide alpha-2,6-sialyltransferase 1	17q25.1	55808
CCM2L	C20orf160; dJ310O13.5	CCM2 like scaffolding protein	20q11.21	140706
FAM167B	C1orf90	Family with sequence similarity 167 member B	1p35.2	84734
MYOM3	-	Myomesin 3	1p36.11	127294
ALS2CL	RN49018	ALS2 C-terminal like	3p21.31	259173
CBX2	M33; CDCA6; SRXY5	Chromobox 2	17q25.3	84733
THBD	TM; THRM; AHUS6	Thrombomodulin	20p11.21	7056
DAG1	A3a; DAG; AGRNR;	Dystroglycan 1	3p21.31	1605
TBC1D7	TBC7; MGCPH; PIG51	TBC1 domain family member 7	6p24.1	51256
CAMKK1	CAMKKA	Calcium/calmodulin dependent protein kinase kinase 1	17p13.2	84254
B4GALT3	β4Gal-T3	β−1,4-galactosyltransferase 3	1q23.3	8703
ARAP3	DRAG1; CENTD3	ArfGAP with RhoGAP domain, ankyrin repeat and PH domain 3	5q31.3	64411
RNASE1	RAC1;RIB1;RNS1	Ribonuclease A family member 1	14q11.2	6035
SYNE3	NET53; Nesp3	Spectrin repeat containing nuclear envelope family member 3	14q32.13	161176
TRIB3	NIPK; SINK; TRB3; SKIP3	Tribbles pseudokinase 3	20p13	57761
ITPR3	IP3R3	Inositol 1,4,5-trisphosphate receptor type 3	6p21.31	3710